Biaxial Failure Surfaces of 2020 and PGX Graphites

F.H. Ho, R.E. Vollman, H. Yu
General Atomic Company, P.O. Box 81608, San Diego, California 92138, U.S.A.
N.R. Adsit
General Dynamics/Convair Division, P.O. Box 80847, San Diego, California 92138, U.S.A.

ABSTRACT

Graphite shows an increase in strength with an increase in temperature, and this characteristic makes graphite a prime candidate for structural applications in the high temperature gas-cooled reactors (HTGR). The core support structure in the HTGR uses high strength graphite. Its ultimate strength under a combined stress state is important for design use. A test program was therefore initiated to determine the multiaxial behavior of two specific types of graphites, in particular the biaxial failure surface which is to be correlated with various failure theories. The two candidate graphites are a fine-grain 2020 (of Stackpole Carbon Company) and a coarse-grain PGX (of Union Carbide Corp).

Tubular specimens are used and are subjected axial loading and internal or external pressure. Various ratios of biaxial stresses are examined but emphasis is placed in the first and fourth stress quadrants.

The tensile fracture pattern reveals a cleavage failure mode. Compressive failure occurs when a limiting value (equivalent to cohesion and internal friction) on any given plane is reached. The maximum stresses at the time of failure are calculated using the thick-wall cylinder formula. A modified Coulomb-Mohr theory with tension-cutoffs proposed by B. Paul (1961) fits the biaxial test data very well. The theory is consistent with the observed fracture patterns and mechanism. The theory appears to give a better correlation with the biaxial test data than the maximum normal stress, maximum shear stress, maximum distortion energy and Tsai and Wu's strength tensor theories.

The failure surfaces obtained are for thin tubular specimen configuration in which the stress state is relatively uniform. The volume and grain size effects are nearly the same. In the application of the failure surfaces to the core support component design, these factors, non-uniform stress state, the volume and grain size effects should be included.

1. Introduction

The failure strength of brittle graphite materials under multiaxial stress states is important for the design of the core support structures in the High Temperature Gas-cooled Reactor (HTGR). Recent studies of this subject have shown that graphite may not conform to the maximum principal stress theory being used tentatively for the graphite structural criteria proposed in ASME III, Division 2 [1].

As part of the investigation to determine what form a multiaxial failure theory should take for use in the ASME Code, a test program has been performed to obtain multiaxial fracture data. The test data will then be used to derive the design strength envelope according to the stress criteria. In addition, it provides data to correlate with various failure theories to establish the one which will best describe the behavior of graphite.

Two candidate graphites, a fine-grained 2020 and a coarse-grained PGX, are examined in this test program. Graphite materials to be characterized are nearly transversely isotropic, therefore it is necessary to obtain a failure surface in the planes perpendicular to and coincident with the isotropic plane. General Dynamics/Convair Division, San Diego, California, performed the test under contract to GA Technologies, Inc.

2. Description of the Test

The application of a general in-plane biaxial state of stress, including tension, compression and shear components, requires the following:

a) A significant volume of material must be under a homogeneous state of stress to minimize strain gradient and grain size effects.

b) Primary failure must start in the gauge section of the specimen.

c) The state of stress/strain must be directly measurable to avoid analytical determination of the stress-strain state.

d) It must be possible to vary the three in-plane stress components independently.

One of the best specimen configurations for the application of a general biaxial state of stress is the thin-walled cylinder. The state of generalized plane stress can be achieved by the independent application of axial loads, internal or external pressure and torque. Since graphite material is brittle, and stress concentrations in the load introduction region and are not relieved by plastic yielding, the biaxial specimen must be very carefully designed. In order to achieve the full potential of the thin-wall tubular specimens, the following requirements must be met:

a) The tube must be loaded without contraints to minimize local extraneous or non-homogeneous stresses.

b) Surface pressures on the material in the test section used for producing circumferential or axial stresses should be minimized to avoid adding a high radial stress component resulting in a triaxial state of stress.

c) Functional or material failures of the load-introduction tabs must be avoided.

d) Undesirable buckling prior to material failure must be avoided.

The general biaxial state of stress is produced by means of internal and external pressures P_i and P_o, longitudinal load P_x and torque T_x about the longitudinal axis.

The current program is limited to the tubular specimens loaded axially with internal or external pressure. No torque is applied. In this way the principal stress axes coincide with the axes of the tubular specimen.

To minimize the grain size effect, the wall thickness of tubes must be of the order of ten grains or larger. The criterion is set to assure that the localized area acts as a multigrained solid rather than a single crystal. This constraint is apparently in conflict with the requirement of a thin-walled cylinder for a homogeneous state of stress. Thus, a compromise is made and specimen configuration is chosen as shown in Fig. 1. The material thickness at the gauge section is 3.8 mm. The maximum grain size of 2020 and PGX graphite are approximately 0.152 and 2.54 mm, respectively.

All the biaxial specimens are machined from the graphite logs with the generator of the tube along the axial direction of the parent log. Three strain gages, two rosettes and one axial gage, are installed at the mid-length and positioned circumferentially 120° apart. The tube surfaces subjected to pressure are all coated to prevent the pressuring medium from intruding into the pores of the graphite. Steel end caps are bonded onto the specimens. These are used to complete the pressure chamber and for axial loading.

3. Test Results

3.1 Fracture Patterns

The fracture patterns of the 2020 and PGX biaxial specimens were individually examined. Five fracture patterns prevailed. The H-patterns indicate the failures by the tensile stress in the hoop direction. The Z-patterns show the failures by the tensile stress in the axial direction. In these two failures modes, the fracture surfaces were found normal to the maximum tensile stress, which are typical cleavage failure. The ZX-patterns reveal the typical compressive failure. Many failures by the compressive stresses were found also in 'CRASH'-mode. These specimens failed into many small pieces.

The fracture patterns of the individual specimens are listed in Tables 1 and 2. Most of the failures are tensile stress failures with H- and Z- patterns.

The fine grained 2020 graphite shows an initially straight crack before any branching occurs. The crack patterns are typical of high energy failure and rapid crack propagation. In the course-grained PGX specimens failure along the grain boundaries can be seen. The crack path is more tortuous and no branching is observed. This is consistent with the thermal stress test results reported in [2] and low energy, low velocity crack propagation.

3.2 Failure Stresses and Strains

The load or stress vs gauge section strain curves for each individual uniaxial or biaxial specimen were obtained. The maximum stress on the inside wall of the tubular specimen was calculated using the classical thick-wall relationships with an axial load imposed.

For the specimens failed in the gauge section the classical formulas give an adequate representation of the maximum stresses.

The hoop and axial strains are obtained from the data on the strain gauges installed on the inside wall of the specimen. The biaxial failure stresses and the failure strains of the 2020 and PGX specimens are summarized in Tables 1 and 2. The uniaxial and biaxial failure stresses for 2020 and PGX graphite are plotted in the biaxial stress plane of Fig. 2. The failure strains are plotted on the biaxial strain plane of Fig. 3.

4. Failure Theory Correlation

4.1 Preliminary Failure Surface Analysis

Preliminary analysis of the failure stress was performed to establish a failure surface with various failure theories. The failure theories considered in that study are the maximum normal stress theory, maximum shear stress theory, maximum distortion energy theory, and Tsai and Wu's strength tensor theory.

A best fit surface corresponding to each failure theory is determined. The resulting best fit failure surfaces corresponding to the four failure theories are shown in Fig. 2.

The maximum normal stress theory and Tsai-Wu theory provide the best correlation with the 2020 and PGX test data, respectively, as can be seen in the figures. However, the degree of correlation is generally not too good. This prompts us to re-examine the test data with other failure theories.

4.2 Discussion on the Biaxial Test Data

An examination of fracture pattern reveals that under tensile stress both 2020 and PGX specimens fractured by cleavage. The maximum normal stress theory should apply in the first (stress) quadrant. This is indeed the case for PGX graphite, see Fig. 4(b). The maximum normal stress theory can even extend partially into the fourth quadrant.

The fit for 2020 graphite data in the first quadrant is not perfect using the maximum normal stress theory. The equi-biaxial tension data points are about 20% lower than the prediction of the maximum normal stress theory. These points are examined in the light of fracture pattern. Half of the specimens failed at or near the ends. Thus the failure stress is underestimated for the equi-biaxial tension case. The maximum normal stress theory can also apply to most of the fourth quadrant as shown in Fig. 4(a).

When the maximum normal stress theory is applied in the first quadrant and partially in the fourth quadrant, the uniaxial strength test results are not considered. This is because the uniaxial test specimen has a different volume and linear dimension (hence grain size effect) [4] than the biaxial test specimen. Therefore only the results of the biaxial test specimens are used in the failure theory correlation.

In the lower part of the fourth quadrant where the compressive stress component is high, the maximum normal stress theory does not fit the data satisfactorily. The fracture pattern appeared to occur through the maximum shear stress. A modified Coulomb-Mohr theory seems to adequately describe the failure.

4.3 Application of the Modified Coulomb-Mohr Theory to the Biaxial Test Data

Following [5] and its notation, one form of the Coulomb-Mohr theory for the failure surface in a three-dimensional stress space is as follows:

$$\sigma_1 = - S_{C1} + \frac{S_{C1}}{S'_{t2}} \sigma_2 \qquad \sigma_1 > \sigma_3 > \sigma_2 \tag{1a}$$

$$\sigma_1 = - S_{C1} + \frac{S_{C1}}{S'_{t3}} \sigma_3 \qquad \sigma_1 > \sigma_2 > \sigma_3 \tag{1b}$$

and etc.

where σ_1, σ_2 and σ_3 are the three principal stresses, and S'_{t1}, S'_{t2} and S'_{t3} are the fictitious uniaxial tensile strengths in the three principal stress directions which would exist, if the Coulomb-Mohr criterion were valid in this range of stresses. The true uniaxial tensile strengths are lower than the fictitious values and will be designated without primes by S_{t1}, S_{t2} and S_{t3}. S_{C1}, S_{C2} and S_{C3} are the uniaxial compressive strengths according to the Coulomb-Mohr criterion.

For a better correlation with experimental data B. Paul [5] suggested the use of tension cutoffs on the Coulomb-Mohr's failure surface for brittle materials. In addition to Eqs. (4) failure occurs also when:

$$\sigma_1 = S_{t1}, \tag{2a}$$

$$\sigma_2 = S_{t2}, \tag{2b}$$

$$\sigma_3 = S_{t3}. \tag{2c}$$

The Coulomb-Mohr's failure surface modified with tension-cutoffs will be used below to correlate with the biaxial data of 2020 and PGX graphites.

Figure 4 shows Coulomb-Mohr's failure surfaces, modified by tension cutoffs on the base of the maximum normal stress theory, for 2020 and PGX graphite, respectively.

5. Conclusions

The following conclusions about the biaxial test data of 2020 and PGX graphites can be made:

1. The modified Coulomb-Mohr theory with tension-cutoffs as proposed by B. Paul [5] appears to give a good correlation with the biaxial test data. This theory fits the 2020 and PGX test data better than many frequently used failure theories.
2. Scarceness of the test data in the second and third quadrants does not warrant an adequate description of the failure surfaces. More data points are needed for a complete failure surface. However, in the interim, one could assume symmetrical failure curve in the stress plane.

References

/1/ Proposed Section III, Division 2, ASME Boiler and Pressure Vessel Code, Subsection CE, Design Requirements for Graphite Core Supports, March, 1982.

/2/ Ho, F. H., and E. Chin, 'Thermal Stress Failure of Artificial Graphite,' presented at the 33rd Pacific Coast Regional Meeting at S. F., American Ceramic Society, October 26-29, 1980.

/3/ Tsai, S. W., and E. M. Wu, 'A General Theory of Strength for Anisotropic Materials,' J. of Composite Material, v. 5, January 1971.

/4/ Ho, F. H., 'A Four Parameter Weibull Theory for the Strength of Granular Brittle Material,' Extended Abstract, 14th Biennial Conf. on Carbon, 1979.

/5/ Paul, B., Macroscopic Criteria for Flow and Fracture, in 'Fracture' edited by H. Liebowitz, Academic Press, 1968.

TABLE 1
BIAXIAL STRENGTH TEST DATA OF 2020 GRAPHITE

Nominal Stress Ratio $\sigma_\theta:\sigma_Z$	No. of Specimen	GAUGE Section σ_θ MPa	σ_x MPa	σ_r MPa	ε_θ %	ε_x %	Failure Pattern*
1:2	4	11.0	22.0	-1.0	.115	.189	Z(4)
1:1	6	18.7	18.7	-1.6	.23	.251	Z(3), T(3)
1:-4	5	18.5	-74.1	-1.6	.31	-1.24	Crashed (5)
-1:-1	3	-87.5	-87.8	0	-1.14	-1.30	Crashed (3)
-6:-1	1	-101.4	-16.5	0	-.55	-.01	Z(1)
-4:-1	3	-54.4	-13.8	0	-.546	-.127	Z(3)
-6.5:1	2	-48.3	7.5	0	-.555	0.182	H(2)
1:0	2	25.1	0	-2.1	.313	-.02	H(2)
2:1	3	23.4	10.7	-2.0	.275	.146	Z(1), T(1), ZX(1)

* Number of specimens in parenthesis.

TABLE 2
BIAXIAL STRENGTH TEST DATA OF PGX GRAPHITE

Nominal Stress Ratio $\sigma_\theta:\sigma_Z$	No. of Specimen	GAUGE Section σ_θ MPa	σ_x MPa	σ_r MPa	ε_θ %	ε_x %	Failure Pattern*
2.2:1	5	9.4	4.3	-0.8	.133	.091	H(5)
1:1	5	8.9	8.5	-0.7	.121	.181	Z(5)
1:2	5	4.55	8.75	-0.4	.081	.192	Z(5)
1:0	5	9.0	0.	-0.8	.127	.018	H(5)
1:-1	3	8.6	8.8	-0.8	.14	-.181	H(3)
1:-4	3	6.3	-26.6	-0.5	.10	-.727	ZX(2), Z(1)
1:-2	3	8.55	17.1	-0.7	.17	-.405	H(3)
0:1	2	0.	9.2	0.	.28	.164	Z(2)

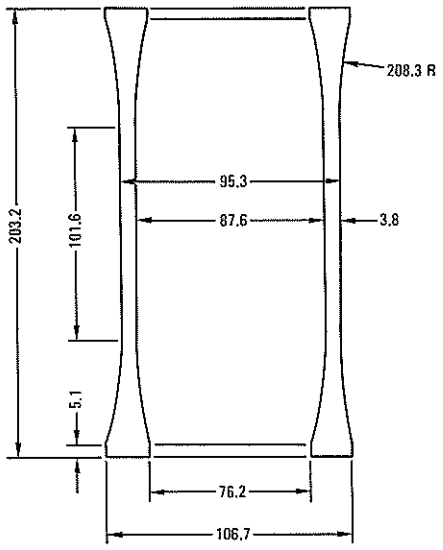

Fig. 1 Biaxial Test Specimen. (All dimensions are in mm.)

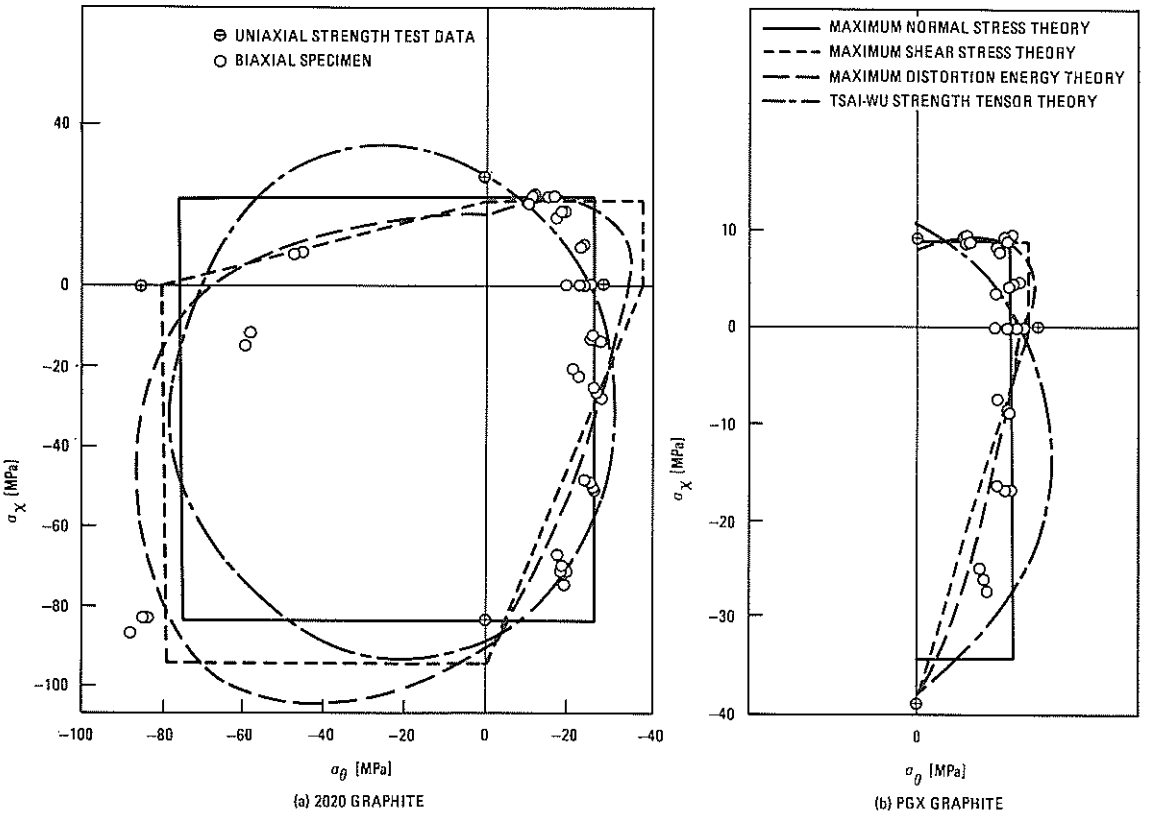

Fig. 2 Biaxial Failure Stress Test Data and Best Fit Failure Surfaces

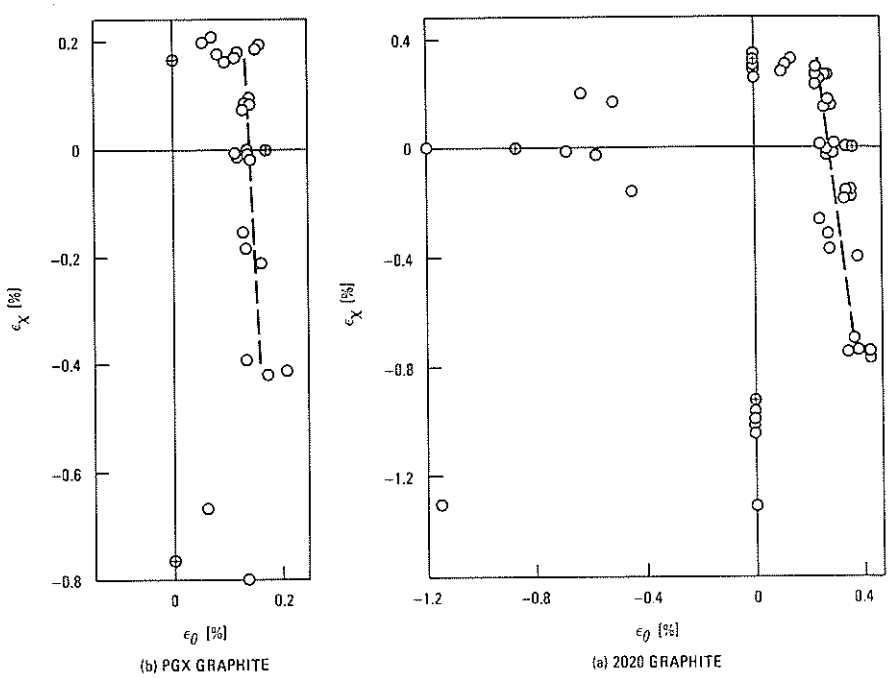

Fig. 3 Biaxial Failure Strains

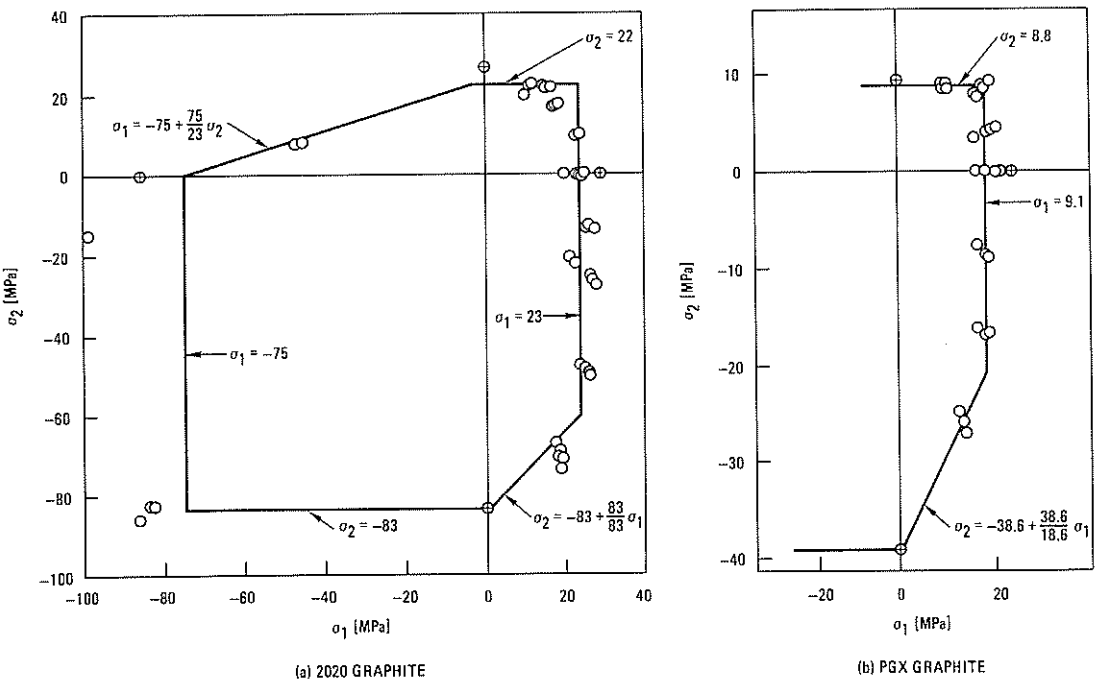

Fig. 4 The Modified Coulomb-Mohr Failure Surface